Torsion of Circular Shaft with Elliptical Inclusions or Cracks

HUANG Cheng[1*], *YIN Maoshu*[2], *QI Xiao*[1], *GUO Hun*[1]

1. School of Aviation and Mechanical Engineering, Changzhou Institute of Technology, Changzhou 213032, P. R. China;
2. Physical Power Division, Shanghai Institute of Space Power-Sources, Shanghai 200240, P. R. China

(Received 14 November 2020; revised 20 January 2021; accepted 1 February 2021)

Abstract: This paper proposes a straightforward and concise approach to analyze the Saint-Venant's torsion of a circular shaft containing multiple elliptical inclusions or cracks based on the complex variable method. The complex potentials are first derived for the shaft with N elliptical inclusions by introducing Faber series expansion, and then the shear stresses and torsional rigidity are calculated. When the inclusions degenerate into cracks, the solutions for the intensity factors of stress are obtained. Finally, several numerical examples are carried out to discuss the effects of geometry parameters, different shear modulus ratios and array-types of the elliptical inclusions/cracks on the fields of stresses. The obtained results show that the proposed approach has advantages such as high accuracy and good convergence.

Key words: Saint-Venant's torsion; complex variable method; Faber series

CLC number: O343.4 **Document code:** A **Article ID:** 1005-1120(2021)01-0096-10

0 Introduction

Circular shafts under torsion are widely used in engineering. To raise the undergoing-load level of the shafts, they are often holed or made into composite shafts reinforced by other materials. Thus, it is of not only theoretical interest but also practical importance to study the torsion of circular shafts containing holes or inclusions.

Ling[1] investigated the Saint-Venant's torsion problem of a circular bar with a ring of uniformly distributed circular holes of equal radii using a special class of harmonic functions introduced by Howland[2]. Kuo et al.[3-4] studied the torsion of a circular tube with circular holes and a cylinder which is reinforced with circular inclusions by constructing a real stress function, respectively. Jaswon et al.[5] proposed an integral equation solution for the classical torsion problem of Saint-Venant through numerically solving a Neumann-type boundary-value equation.

The solution for torsion problem of a circular shaft can always be solved by using numerical techniques[6-11]. Katsikadelis et al.[7] presented the boundary element solution for the Saint-Venant torsion problem of composite cylindrical bars of arbitrary cross section. Spountzakis et al.[8] developed the boundary element method for the nonuniform torsion of composite bars of arbitrary constant cross section by using domain discretization and an effective Gaussian integration over domains of arbitrary shape. Li et al.[9] studied the Saint-Venant's torsion problem of the arbitrarily shaped bar made of different materials based on finite element method. Refs. [10-11] adopted the null-field approach to solve the Saint-Venant's problem of a circular bar with circular holes or inclusions, respectively.

Recently, the research on torsion of advanced materials has attracted extensive attention. Ecsedi et al.[12] generalized the known elastic solution of Saint-Venant's torsional problem developed by Prandtl to piezoelectric beams, and later they investigated the Saint-Venant torsion of non-homogeneous and circular cylinder made of orthotropic

*Corresponding author, E-mail address: huangcheng@czu.cn.

How to cite this article: HUANG Cheng, YIN Maoshu, QI Xiao, et al. Torsion of circular shaft with elliptical inclusions or cracks[J]. Transactions of Nanjing University of Aeronautics and Astronautics, 2021, 38(1): 96-105.

http://dx.doi.org/10.16356/j.1005-1120.2021.01.009

piezoelectric material[13]. Wang et al.[14] studied the effects of surface elasticity in the Saint-Venant torsion problem. Hassani et al.[15] analyzed the Saint-Venant torsion of an orthotropic bar with multiple curved cracks. However, it should be noted that the above work was all made by real variable method.

Muskhelishvili[16] developed a complex variable method to address the Saint-Venant's torsion of composite circular shafts and solved the problem of a circular shaft containing an eccentric circular inclusion. Based on the Muskhelishvili's method, Yue et al.[17] dealt with the torsion problem of a composite cylinder with cracks and inclusions by introducing the Mellin transforms and solving a set of mixed-type integral equations. Refs.[18-19] showed that, based on the complex variable method, the interaction between porous/inclusions can be effectively solved. However, to the author's knowledge, no work can be found for the solution to the Saint-Venant's torsion of a circular shaft containing multiple elliptical inclusions based on the complex variable method.

In this paper, we propose a straightforward and concise approach to analyze the problem of interacting elliptical inclusions in a circular shaft of torsion based on complex variable theory. The key step in the present work is to express the complex potentials in the matrix with elliptical holes (a multiply-connected region) in the form of Faber series, and then the continuous conditions between the inclusions and the matrix are used to determine the unknown coefficients involved in these complex potentials. Thus, the novel feature of this paper is to present a straightforward and concise method to solve the problem of the Saint-Venant's torsion of a circular shaft containing multiple elliptical inclusions or cracks effectively with high accuracy.

1 Basic Equations

In a rectangular coordinate system x-y-z, consider a circular shaft containing N elliptical inclusions which are parallel to each other along the z direction. The cross-section of the shaft is shown in Fig.1, where a_p and b_p ($p=1,2,\cdots,N$) are the lengths of the elliptical inclusions' semi-axis, and z_{p0} are the center coordinates of inclusions, respectively. All the inclusions are assumed to be completely bounded to the matrix. The boundaries of the inclusions and the outer contour of the shaft are denoted by L_k ($k=0,1,2,\cdots,N$). We now study Saint-Venant torsion problem of the composite shaft loaded by the torque T applied at its two ends.

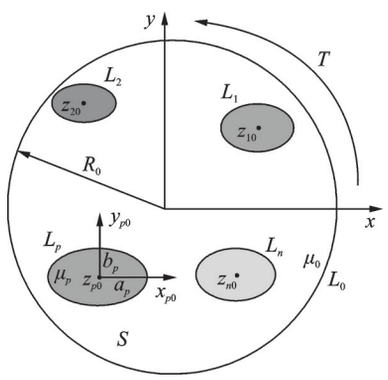

Fig.1 Torsion of a circular shaft containing multiple elliptical inclusions

In this case, the components of displacement (u, v, w) can be expressed as

$$u=-\tau zy,\quad v=\tau zx,\quad w=\tau\varphi(x,y) \tag{1}$$

where τ is the angle of twist per unit length along the z direction and $\varphi(x,y)$ the warping function. The corresponding stresses are

$$\begin{cases}\sigma_x=0,\quad \sigma_y=0,\quad \sigma_z=0,\quad \sigma_{xy}=0\\ \sigma_{xz}=\mu_k\tau\left(\dfrac{\partial\varphi}{\partial x}-y\right)\\ \sigma_{yz}=\mu_k\tau\left(\dfrac{\partial\varphi}{\partial y}+x\right)\quad k=0,1,2,\cdots,N\end{cases} \tag{2}$$

where μ_0 is the shear modulus of the matrix, and μ_k ($k=1,2,\cdots,N$) are the shear modulus of the k-th inclusion. For this problem, the equilibrium equation becomes that[16]

$$\frac{\partial\sigma_{xz}}{\partial x}+\frac{\partial\sigma_{yz}}{\partial y}=0 \tag{3}$$

where the body force is neglected. Substituting Eq.(2) into Eq.(3) leads to the Laplace equation

$$\frac{\partial^2\varphi}{\partial^2 x}+\frac{\partial^2\varphi}{\partial^2 y}=0 \tag{4}$$

The solution of Eq.(4) is

$$\varphi = \mathrm{Re}\,[F(z)] \quad z = x + \mathrm{i}y \tag{5}$$

where $F(z)$ is called as the complex potential. Substituting Eq.(5) into Eqs.(1—2), the displacement and stress can finally be expressed as[16]

$$w = \frac{1}{2}\tau\,[F(z) + \overline{F(z)}] \tag{6}$$

$$\sigma_{xz} - \mathrm{i}\sigma_{yz} = \mu_k \tau (F'(z) - \mathrm{i}\bar{z}) \tag{7}$$

Once $F(z)$ is obtained, the torsional rigidity D can be calculated by[16]

$$D = \frac{T}{\tau} = \sum_{k=0}^{N} \mu_k \iint \left(x^2 + y^2 + x\frac{\partial \varphi}{\partial y} - y\frac{\partial \varphi}{\partial x} \right) \mathrm{d}x\mathrm{d}y \tag{8}$$

To solve $F(z)$, we introduce the resultant traction p on any boundary as

$$p = \int_s \sigma_{zx}\mathrm{d}y - \sigma_{zy}\mathrm{d}x \tag{9}$$

Inserting Eq.(7) into Eq.(9) leads to

$$p = \frac{\mu_k \tau}{2\mathrm{i}}\,[F(z) - \overline{F(z)} - \mathrm{i}z\bar{z} + C_0] \tag{10}$$

where C_0 is a constant and it can be assumed to be zero without affecting the stresses. Since there is no external traction on the cylindrical surface, $p = 0$ and the boundary condition on L_0 can be derived from Eq.(10) that

$$F_0(z) - \overline{F_0(z)} - \mathrm{i}z\bar{z} = 0 \tag{11}$$

where the subscripts "0" denote the matrix. At the interface between the matrix and inclusions L_k ($k = 0, 1, 2, \cdots, N$), the continuity conditions require that

$$w_0 = w_k \tag{12}$$

$$p_0 = p_k \tag{13}$$

where w_k and p_k stand for the displacement and resultant traction along the kth inclusion's boundary, respectively. Substituting Eqs.(6,10) into Eqs.(12, 13), we have

$$F_0(z) + \overline{F_0(z)} = F_k(z) + \overline{F_k(z)} \tag{14}$$

$$(F_0(z) - \overline{F_0(z)}) - g_k(F_k(z) - \overline{F_k(z)}) - \mathrm{i}(1 - g_k)z\bar{z} + C_k = 0 \tag{15}$$

where $g_k = \mu_k/\mu_0$ ($k = 1, 2, \cdots, N$) denotes the shear modulus ratios, and C_k ($k = 1, 2, \cdots, N$) the constants to be determined.

2 Theoretical Analyses

In this case, the matrix is a multiple-connected region containing N elliptic holes and enclosed by the circle, so the complex potential in the matrix has the form that

$$F_0(z) = f_0(z) + \sum_{k=1}^{N} f_k(z) \tag{16}$$

where $f_0(z)$ is an analytical function inside L_0, and $f_k(z)$ is another analytical function outside the elliptical hole L_k. Thus $f_0(z)$ can be expanded into the Taylor series as

$$f_0(z) = \sum_{j=0}^{\infty} A_j \left(\frac{z}{R_0} \right)^j \tag{17}$$

where A_j are unknown coefficients. Introduce the following conformal mapping function

$$z - z_{k0} = \omega(\xi_k) - z_{k0} = R_k \left(\xi_k + \frac{m_k}{\xi_k} \right) \tag{18}$$

$$R_k = \frac{a_k + b_k}{2}, m_k = \frac{a_k - b_k}{a_k + b_k} \tag{19}$$

which conformably maps the region outside the elliptical hole L_k onto the external region of a unit circle of $\xi_k = \mathrm{e}^{\mathrm{i}\theta}$ in the ξ_k-plane, and thus $f_k(z)$ can be expanded into the Laurent series as

$$f_k(z) = \sum_{j=0}^{\infty} B_j^{(k)} \xi_k^{-j}(z) \tag{20}$$

where $B_j^{(k)}$ are unknown coefficients. Inserting Eqs.(17,20) into Eq.(16) yields that

$$F_0(z) = \sum_{j=0}^{\infty} A_j \left(\frac{z}{R_0} \right)^j + \sum_{k=1}^{N} \sum_{j=0}^{\infty} B_j^{(i)} \xi_k^{-j}(z) \tag{21}$$

On the surface of the shaft L_0, $z = R_0 \mathrm{e}^{\mathrm{i}\theta} = R_0\sigma$ and thus Eq.(21) has the form that

$$F_0(\sigma) = \sum_{j=0}^{\infty} A_j \sigma^j + \sum_{k=1}^{N} \sum_{j=0}^{\infty} B_j^{(k)} \xi_k^{-j}(\sigma) \tag{22}$$

On the other hand, $\xi_k^{-j}(\sigma)$ can be expanded into the complex Fourier series on the unit circle as

$$\xi_k^{-j}(\sigma) = \sum_{n=-\infty}^{\infty} \beta_{kjn}^{(0)} \sigma^n \tag{23}$$

$$\beta_{kjn}^{(0)} = \frac{1}{2\pi} \int_{-\pi}^{\pi} \xi_k^{-j} \sigma^{-n} \mathrm{d}\theta \tag{24}$$

where the unknown function $\xi_k^{-1}\left(\left|\xi_k^{-1}\right| < 1\right)$ can be determined from Eq.(18) as

$$\xi_k^{-1}=\frac{z-z_{k0}}{2R_km_k}-\sqrt{\left(\frac{z-z_{k0}}{2R_km_k}\right)^2-\frac{1}{m_k}} \tag{25}$$

which can be used to determine the coefficients by Eq.(24). Substituting Eq.(22) into Eq.(11), after some rearrangement, we can get that

$$\sum_{j=0}^{\infty}A_j\sigma^j+\sum_{k=1}^{N}\sum_{j=0}^{\infty}\sum_{n=-\infty}^{\infty}B_j^{(k)}\beta_{kjn}^{(0)}\sigma^n-\left(\sum_{j=0}^{\infty}\overline{A}_j\sigma^{-j}+\sum_{k=1}^{N}\sum_{j=0}^{\infty}\sum_{n=-\infty}^{\infty}\overline{B_j^{(k)}}\,\overline{\beta_{kjn}^{(0)}}\sigma^{-n}\right)=\mathrm{i}R_0^2 \tag{26}$$

On the other hand, for any inclusion $L_p(p=1,2,\cdots,N)$, moving the origin of the global system $x-y$ in to the point z_p, that is, making the following coordinate translation: $z-z_p=z^*$, one can express the complex potential in the matrix and inside the inclusions, in the local coordinate system x_p-y_p, as

$$F_0(z^*)=\sum_{j=0}^{\infty}A_j\left(\frac{z^*+z_p}{R_0}\right)^j+\sum_{j=0}^{\infty}B_j^{(p)}\xi_p^{-j}(z^*)+\sum_{\substack{k=1\\k\neq p}}^{N}\sum_{j=0}^{\infty}B_j^{(k)}\xi_k^{-j}(z^*) \tag{27}$$

$$F_p(z^*)=\sum_{j=0}^{\infty}c_j^{(p)}\left(\xi_p^j(z^*)+m_p^j\xi_p^{-j}(z^*)\right) \tag{28}$$

where $c_j^{(p)}$ are unknown coefficients. In Eq.(27), we define $\xi_0^j(z^*)=\left((z^*+z_p)/R_0\right)^j$, and it can be expanded into the complex Fourier series as

$$\xi_0(z^*)=\frac{R_p(\sigma+m_p\sigma^{-1})+z_{p0}}{R_0} \tag{29}$$

$$\xi_0^j(z^*)=\sum_{n=-\infty}^{\infty}\beta_{0jn}^{(p)}\sigma^n \tag{30}$$

$$\beta_{0jn}^{(p)}=\frac{1}{2\pi}\int_{-\pi}^{\pi}\xi_0^j(z^*)\,\sigma^{-n}\mathrm{d}\theta \tag{31}$$

From Eqs.(29—31), we can obtain the coefficients $\beta_{0jn}^{(p)}$. In Eq.(27), the term $\xi_k^{-j}(z^*)$ is a given function that is analytic inside the inclusion $L_p(p\neq k)$, and thus it can be expanded into the Faber series as[20-21]

$$\xi_k^{-j}(z^*)=\sum_{n=0}^{\infty}A_{kjn}^{(p)}P_n^{(p)}(z^*) \tag{32}$$

$$P_n^{(p)}(z^*)=\xi_k^n+m_p^n\xi_k^{-n} \tag{33}$$

$$A_{k1n}^{(p)}=\frac{1}{2\pi}\int_0^{2\pi}\xi_k^{-1}(z^*)\,\mathrm{e}^{-\mathrm{i}n\theta}\mathrm{d}\theta \tag{34}$$

where the known function $\xi_k^{-1}\left(\left|\xi_k^{-1}\right|<1\right)$ can be determined as

$$\xi_k^{-1}(z^*)=d_1+d_2-\sqrt{(d_1+d_2)^2-\frac{1}{m_k}} \tag{35}$$

$$d_1=\frac{z_{p0}-z_{k0}}{2R_km_k},\ d_2=\frac{R_p\left(\sigma+\dfrac{m_p}{\sigma}\right)}{2R_km_k} \tag{36}$$

After the coefficients $A_{k1n}^{(p)}$ are obtained from Eqs.(34, 35), the coefficients $A_{kjn}^{(p)}$ in Eq.(32) can be easily calculated by using the following recurrence relations[22]

$$A_{k,(j+1),n}^{(p)}=\sum_{s=0}^{n}A_{k,j,n-s}^{(p)}A_{k,1,s}^{(p)}+\sum_{s=1}^{n}m_p^s\left(A_{k,j,s}^{(p)}A_{k,1,n+s}^{(p)}+A_{k,j,n+s}^{(p)}A_{k,1,s}^{(p)}\right) \tag{37}$$

Inserting Eqs.(27,28) into Eqs.(14,15) yields that

$$\begin{aligned}&\sum_{j=0}^{\infty}A_j\sum_{n=-\infty}^{\infty}\beta_{0jn}^{(p)}\sigma^n+\sum_{j=0}^{\infty}B_j^{(p)}\sigma^{-j}+\sum_{\substack{k=1\\k\neq p}}^{N}\sum_{j=0}^{\infty}B_j^{(k)}\sum_{n=0}^{\infty}A_{kjn}^{(p)}P_n^{(p)}(\sigma)+\left(\sum_{j=0}^{\infty}\overline{A}_j\sum_{n=-\infty}^{\infty}\overline{\beta_{0jn}^{(p)}}\sigma^{-n}+\right.\\&\left.\sum_{j=0}^{\infty}\overline{B_j^{(p)}}\sigma^j+\sum_{\substack{k=1\\k\neq p}}^{N}\sum_{j=0}^{\infty}\overline{B_j^{(k)}}\sum_{n=0}^{\infty}\overline{A_{kjn}^{(p)}}\,\overline{P_n^{(p)}(\sigma)}\right)=\\&\sum_{j=0}^{\infty}C_j^{(p)}(\sigma^j+m_p^j\sigma^{-j})+\sum_{j=0}^{\infty}\overline{C_j^{(p)}}\,(\sigma^{-j}+m_p^j\sigma^j)\end{aligned} \tag{38}$$

$$\begin{aligned}&\sum_{j=0}^{\infty}A_j\sum_{n=-\infty}^{\infty}\beta_{0jn}^{(p)}\sigma^n+\sum_{j=0}^{\infty}B_j^{(p)}\sigma^{-j}+\sum_{\substack{k=1\\k\neq p}}^{N}\sum_{j=0}^{\infty}B_j^{(k)}\sum_{n=0}^{\infty}A_{kjn}^{(p)}P_n^{(p)}(\sigma)-\left(\sum_{j=0}^{\infty}\overline{A}_j\sum_{n=-\infty}^{\infty}\overline{\beta_{0jn}^{(p)}}\sigma^{-n}+\right.\\&\left.\sum_{j=0}^{\infty}\overline{B_j^{(p)}}\sigma^j+\sum_{\substack{k=1\\k\neq p}}^{N}\sum_{j=0}^{\infty}\overline{B_j^{(i)}}\sum_{n=0}^{\infty}\overline{A_{kjn}^{(p)}}\,\overline{P_n^{(p)}(\sigma)}\right)-\\&g_p\left[\sum_{j=0}^{\infty}C_j^{(p)}(\sigma^j+m_p^j\sigma^{-j})-\sum_{j=0}^{\infty}\overline{C_j^{(p)}}\,(\sigma^{-j}+m_p^j\sigma^j)\right]=\\&\mathrm{i}(1-g_p)\left[R_p\left(\sigma+\frac{m_p}{\sigma}\right)+z_{p0}\right]\cdot\\&\left[R_p\left(\frac{1}{\sigma}+\sigma m_p\right)+\overline{z_{p0}}\right]-C_p\end{aligned} \tag{39}$$

where $P_n^{(p)}=\sigma^n+m_p^n\sigma^{-n}$. Comparison of the coefficients of $\sigma^{\pm m}(m\geqslant 1)$ at the two sides of Eqs.(26, 37,38) yields that

$$A_m+\sum_{k=1}^{N}\sum_{j=1}^{\infty}B_j^{(k)}\beta_{kjm}^{(0)}-\sum_{k=1}^{N}\sum_{j=1}^{\infty}\overline{B_j^{(k)}}\,\overline{\beta_{kj(-m)}^{(0)}}=0 \quad (40)$$

$$\overline{A_m}+\sum_{k=1}^{N}\sum_{j=1}^{\infty}\overline{B_j^{(k)}}\,\overline{\beta_{kjm}^{(0)}}-\sum_{k=1}^{N}\sum_{j=1}^{\infty}B_j^{(k)}\beta_{kj(-m)}^{(0)}=0 \quad (41)$$

$$\sum_{j=1}^{\infty}A_j\beta_{0jm}^{(p)}+\sum_{\substack{k=1\\k\neq p}}^{N}\sum_{j=1}^{\infty}B_j^{(k)}A_{kjm}^{(p)}+\sum_{j=1}^{\infty}\overline{A_j}\,\overline{\beta_{oj(-m)}^{(p)}}+\overline{B_m^{(p)}}+\sum_{\substack{k=1\\k\neq p}}^{N}\sum_{j=1}^{\infty}\overline{B_j^{(k)}}\,\overline{A_{kjm}^{(p)}}\,m_p^m=C_m^{(p)}+\overline{C_m^{(p)}}\,m_p^m \quad (42)$$

$$\sum_{j=1}^{\infty}\overline{A_j}\,\overline{\beta_{0jm}^{(p)}}+\sum_{\substack{k=1\\k\neq p}}^{N}\sum_{j=1}^{\infty}\overline{B_j^{(k)}}\,\overline{A_{kjm}^{(p)}}+\sum_{j=1}^{\infty}A_j\beta_{oj(-m)}^{(p)}+B_m^{(p)}+\sum_{\substack{k=1\\k\neq p}}^{N}\sum_{j=1}^{\infty}B_j^{(k)}A_{kjm}^{(p)}m_p^m=\overline{C_m^{(p)}}+m_p^mC_m^{(p)} \quad (43)$$

$$\sum_{j=1}^{\infty}A_j\beta_{0jm}^{(p)}+\sum_{\substack{k=1\\k\neq p}}^{N}\sum_{j=1}^{\infty}B_j^{(k)}A_{kjm}^{(p)}-\sum_{j=1}^{\infty}\overline{A_j}\,\overline{\beta_{oj(-m)}^{(p)}}-\overline{B_m^{(p)}}-\sum_{\substack{k=1\\k\neq p}}^{N}\sum_{j=1}^{\infty}\overline{B_j^{(k)}}\,\overline{A_{kjm}^{(p)}}\,m_p^m-g_p(C_m^{(p)}-\overline{C_m^{(p)}}\,m_p^m)=\delta \quad (44)$$

$$\sum_{j=1}^{\infty}\overline{A_j}\,\overline{\beta_{0jm}^{(p)}}+\sum_{\substack{k=1\\k\neq p}}^{N}\sum_{j=1}^{\infty}\overline{B_j^{(k)}}\,\overline{A_{kjm}^{(p)}}-\sum_{j=1}^{\infty}A_j\beta_{oj(-m)}^{(p)}-B_m^{(p)}-\sum_{\substack{k=1\\k\neq p}}^{N}\sum_{j=1}^{\infty}B_j^{(k)}A_{kjm}^{(p)}m_p^m-g_p(\overline{C_m^{(p)}}-m_p^mC_m^{(p)})=\overline{\delta} \quad (45)$$

where $m=1,2,\cdots,M$ and

$$\delta=\begin{cases}\mathrm{i}(1-g_p)(R_p\bar{z}_{p0}+R_pz_{p0}m_p) & m=1\\ \mathrm{i}(1-g_p)(R_p^2m_p) & m=2\\ 0 & m\geqslant 3\end{cases} \quad (46)$$

In detail, a system of linear equations with respect to the unknown coefficients A_j, $\bar{A}_j$, $B_j^{(k)}$, $\bar{B}_j^{(k)}$, $C_j^{(k)}$, $\bar{C}_j^{(k)}$ ($k=1,2,\cdots,N;j=1,2,\cdots,M$) can be obtained by equating the corresponding coefficients on the two sides of Eqs.(40—45). In addition, $C_m(m\neq 0)$ can be determined by equaling the constant terms on the two sides of Eq.(39), but they have no influence on stresses, and thus are ignored.

Once all the complex coefficients are determined from these linear equations, the stresses both in the matrix and the inclusions can be obtained by[16]

$$\sigma_\rho-\mathrm{i}\sigma_\theta=\frac{\mu_0\tau\xi}{|\omega'(\xi)|}[(F_0(\xi))'-\mathrm{i}\overline{\omega(\xi)}\omega'(\xi)] \quad (47)$$

At the same time, the torsional rigidity can be easily determined by

$$D=D_0+\sum_{k=1}^{N}D_k \quad (48)$$

where

$$D_0=\frac{\mu_0}{4\mathrm{i}}\sum_{j=0}^{N}\int_{L_j}\overline{\omega^2(\xi)}\omega(\xi)\mathrm{d}\omega(\xi)-\frac{\mu_0}{2}\sum_{j=0}^{N}\int_{L_j}\mathrm{Re}[F(\xi)]\mathrm{d}[\overline{\omega(\xi)}\omega(\xi)] \quad (49)$$

$$D_k=\frac{\mu_k}{4\mathrm{i}}\int_{L_j}\overline{\omega^2(\xi)}\omega(\xi)\mathrm{d}\omega(\xi)-\frac{\mu_k}{2}\int_{L_j}\mathrm{Re}[F(\xi)]\mathrm{d}[\overline{\omega(\xi)}\omega(\xi)] \quad (50)$$

If one assumes $\mu_k=0$, and the short-axis radius of the ellipse $b_k=0$, thus the inclusion L_k degenerates into a crack parallel to the x-axis. In this case one can calculate the stress intensity factor for the shaft with the crack by[16]

$$K_{\mathrm{III}}=\lim_{\xi\to\xi_0}\left|\sqrt{2[\omega(\xi)-\omega(\xi_0)]}\right|\cdot\tau \quad (51)$$

where ξ_0 is the point at the unit circle of ξ plane, and it is corresponding to the tip of the crack in the z-plane. Substituting Eq.(18) into Eq.(51), we finally have

$$K_{\mathrm{III}}=\frac{1}{\left|\sqrt{\omega''(\xi_0)}\right|}\{-\mathrm{Im}[\mu_0\tau\xi_0F'(\xi_0)]\} \quad (52)$$

3 Numerical Results and Discussion

3.1 Torsion of a circular shaft containing a circular inclusion

In order to show validity of the present method, we make some comparisons with the related work in Ref.[11], which considered a circular shaft of radius containing a circular inclusion, as shown in Fig.2. In the example we take the ratio of $R_1/R_2=0.3$, $l/R_0=0.6$ and the shear modulus ratio $g_1=\mu_1/\mu_0=0.6$. The numerical results for the non-dimensional torsional rigidity $D^*=2D/(\mu_0\pi R_0^4)$ versus the number of power series terms are shown in Fig. 3. It is shown that the results are accurate enough when the numbers of power series terms are above five. Furthermore, the variations of D^* as functions of the shear modulus ratio g_1 are shown in Table 1, where results in Refs.[16,17] using the in-

tegral formulation and in Ref.[11] based on the null-field integral approach are also listed. It can be seen that the results obtained in the present work are well consistent with those in the previous works.

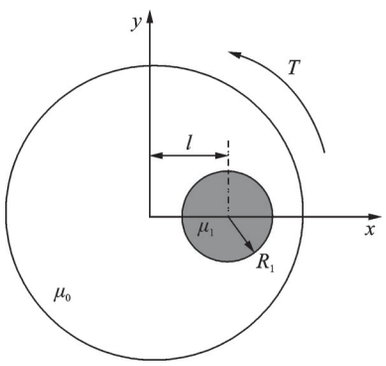

Fig.2 Torsion of a circular shaft containing a circular inclusion

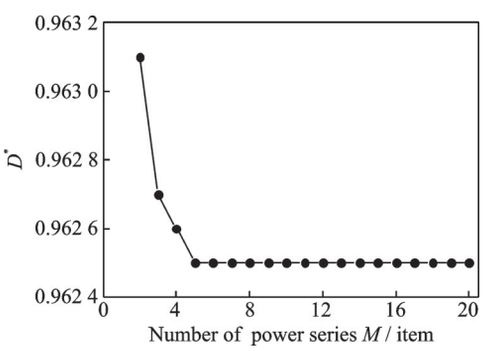

Fig.3 Torsional rigidity versus the number of power series terms

Table 1 Torsional rigidity of a circular shaft containing a circular inclusion

g_1	D^*			
	Ref.[16]	Ref.[17]	Ref.[11]	Present method
0	0.823 70	0.823 77	0.823 70	0.823 70
0.6	0.962 46	0.962 46	0.962 46	0.962 46
1	1.000 00	1.000 00	1.000 00	1.000 00
20	1.252 24	1.251 81	1.252 24	1.252 24
1 000	9.198 66	N/A	9.198 66	9.198 65
1 000 000	8 101.100 12	N/A	8 101.098 83	8 101.093 44

3.2 Torsion of a circular shaft containing multiple circular inclusions

Consider the case of four circular inclusions located in a rhombic array, as shown in Fig.4. For comparison with previous work, we take the same parameters as those in Refs.[3, 4, 11] as follows: $l/R_0 = 0.6$, $g_k = 29.4$ and $R_k/R_0 = 0.25$ ($k = 1, 2, 3, 4$). The results of the non-dimensional torsional rigidity D^* are shown in Table 2, and it is shown that the present solutions are in very agreement with the work in Ref.[11], and more accurate than the results in Refs.[3,4].

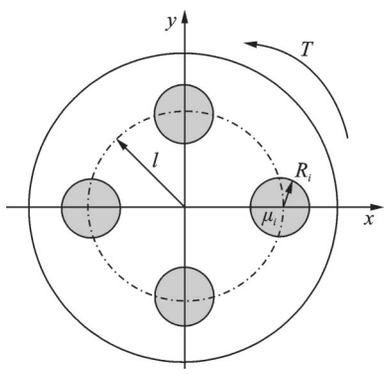

Fig.4 Torsion of a circular shaft containing four circular inclusions of equal radii

Table 2 Torsional rigidity of a circular shaft containing four circular inclusions

Parameter	Refs.[3,4]	Ref.[11]	Present result
D^*	1.570 6	1.774 0	1.774 045

As special cases, the torsion of a circular shaft containing three circular holes of equal radii is also given, as shown in Fig.5, where $l/R_0 = 0.6$, $g_k = 0$ and $R_k/R_0 = 0.2 (k = 1, 2, 3)$. When taking the series expansion as $M = 20$, the shear stresses along the boundaries are shown in Table 3, and it can be found that the present solutions are well consistent with the results in Ref.[1].

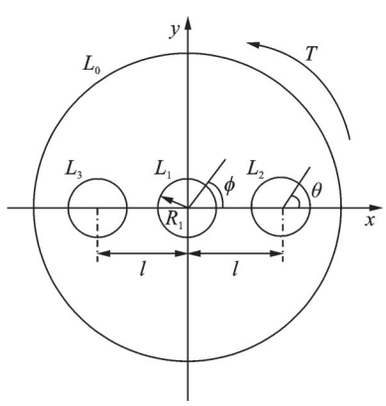

Fig.5 Torsion of a circular shaft containing three circular holes of equal radii

Table 3 Shear stresses $\sigma_\theta/\mu\tau R_0$ along the boundaries (M=20)

θ	L_0 (Exterior boundary)		L_1 (Central hole)		L_2 (Eccentric holes)	
	Ref.[1]	Present result	Ref.[1]	Present result	Ref.[1]	Present result
0	1.308	1.307 8	0.459	0.458 9	1.547	1.546 7
$\pi/6$	0.967	0.966 4	0.277	0.277 0	1.327	1.327 3
$\pi/3$	0.928	0.928 2	0.081	0.080 7	0.793	0.792 5
$\pi/2$	0.932	0.932 4	0.026	0.025 8	0.145	0.145 1
$2\pi/3$	0.928	0.928 2	0.081	0.080 7	−0.451	−0.450 8
$5\pi/6$	0.967	0.966 4	0.277	0.277 0	−0.871	−0.870 8
π	1.308	1.307 8	0.459	0.458 9	−1.033	−1.033 3

3.3 Torsion of a circular shaft containing multiple elliptical inclusions

Consider the case of the circular shaft with two elliptical inclusions, as shown in Fig.6, where $a_1 = a_2 = 0.2R_0$, $b_1 = b_2$ as variables, $l/R_0 = 0.6$, and $\mu_k = \mu(k = 1, 2)$. When $g = \mu/\mu_0 > 1$, the inclusions are called as hard inclusions, and when $g < 1$, they are called as soft inclusions. Specially, when $g = 0$, the inclusion becomes an elliptic hole. The non-dimensional torsional rigidity D^* for different values of b_1/a_1 is shown in Fig.7, which shows that for the soft inclusions, the torsional rigidity greatly decreases as the inclusions become softer, and for the hard inclusions, the torsional rigidity greatly increases as the inclusions become harder. On the other hand, the stresses at the interface between the matrix and the inclusions are shown in Figs.8—10 for three different cases. It is found from Fig.8 that when $g = 0$, the greatest stress occurs at the points on the hole's boundary nearest to the exterior surface of the shaft. Fig.9 is the case of the shaft with two soft elliptic inclusions ($g = 0.5$), and it is found that the maximum stress σ_θ along the surface be-

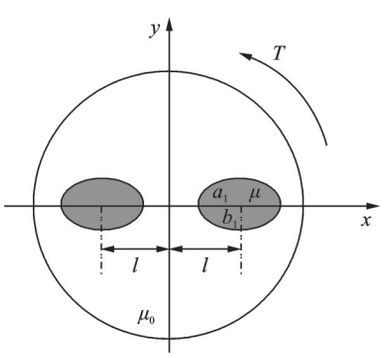

Fig.6 Torsion of a circular shaft containing two elliptical inclusions

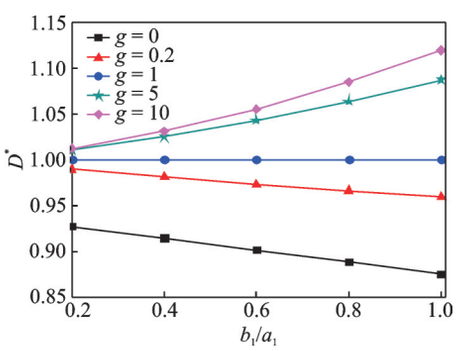

Fig.7 Non-dimensional torsional rigidity D^* versus b_1/a_1

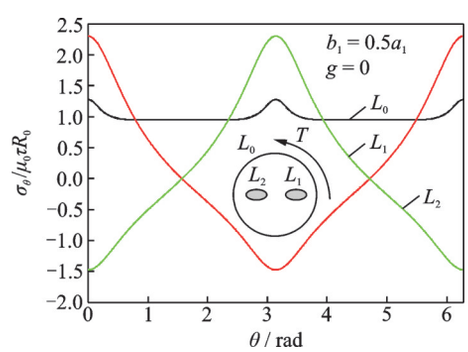

Fig.8 Shaft with two elliptic holes: Stress along the boundaries of the shaft and holes

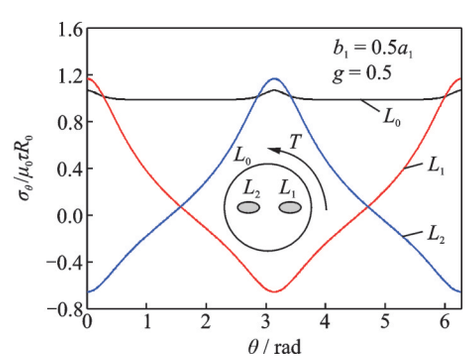

Fig.9 Shaft with two soft elliptic inclusions: Stress along the boundaries of the shaft and inclusions

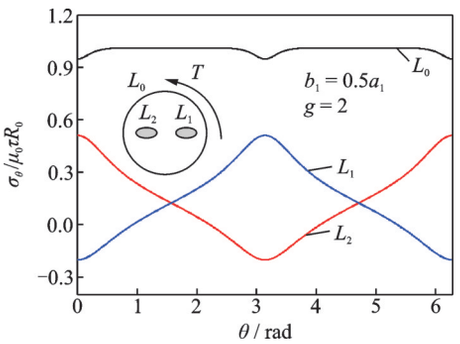

Fig.10 Shaft with two hard elliptic inclusions: Stress along the boundaries of the shaft and inclusions

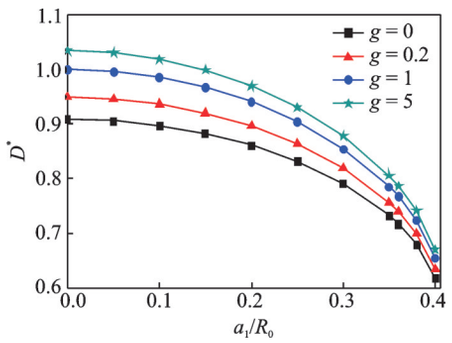

Fig.12 Non-dimensional torsional rigidity D^* versus a_1/R_0

tween the matrix and inclusions decreases compared with that in the case of $g=0$. However, for the case of two hard inclusions, the maximum value of the stress occurs on the exterior surface of the shaft rather than at the boundary of the inclusions, as shown in Fig.10.

3.4 Torsion of a circular shaft containing multiple elliptical inclusions and cracks

Consider the case of the circular shaft with two elliptical inclusions and two cracks shown in Fig.11, where $a_1=a_2$ as variables, $a_3=a_4=0.1R_0$, $b_1=b_2=0$, $b_3=b_4=0.2R_0$, $l/R_0=0.6$, $\mu_1=\mu_2=0$, $\mu_3=\mu_4=\mu$. The non-dimensional torsional rigidity D^* for different values of a_1/R_0 are shown in Fig.12, which shows that with the larger ratio of a_1/R_0, the loss of relative D^* changes greater. Owing to its geometrical symmetry, we just discuss the stress intensity factors of the crack on the right of the circular. Therefore, the non-dimensional stress intensity factors $K_{\mathrm{III}}^*(c)=\left|K_{\mathrm{III}}(c)\Big/(\mu_0\tau R_0\sqrt{a_1}\,D^*)\right|$ and $K_{\mathrm{III}}^*(d)=\left|K_{\mathrm{III}}(d)\Big/(\mu_0\tau R_0\sqrt{a_1}\,D^*)\right|$ for different values of a_1/R_0 are shown in Fig.13. It is shown that with the increase of the g, the variation of the stress intensity factor $K_{\mathrm{III}}^*(c)$ is larger than that of $K_{\mathrm{III}}^*(d)$, and as the crack length becomes large, the $K_{\mathrm{III}}^*(d)$ sharply increases while the $K_{\mathrm{III}}^*(c)$ decreases slowly.

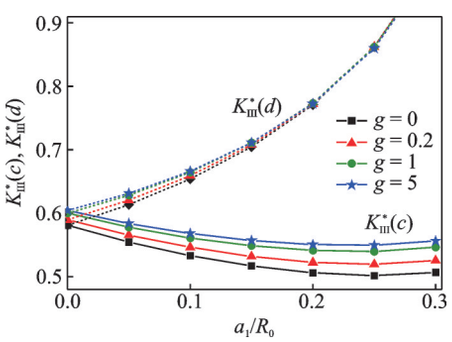

Fig.13 Non-dimensional intensity factor $K_{\mathrm{III}}^*(c)$ and $K_{\mathrm{III}}^*(d)$ versus a_1/R_0

As a special case, the solutions for the torsion of a circular shaft containing a center circular hole and a crack, as shown in Fig.14, are also given. In the example, we take $R_1/R_0=0.2$, and $l/R_0=$

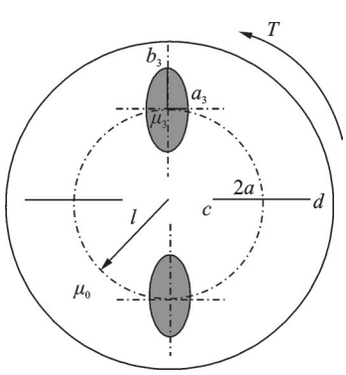

Fig.11 Torsion of a circular shaft containing two elliptical inclusions and cracks

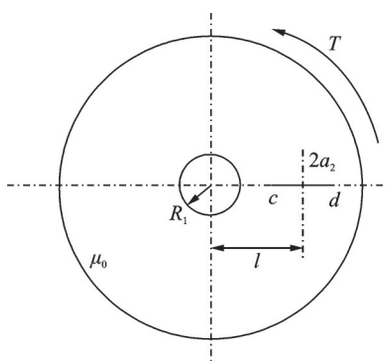

Fig.14 Torsion of a circular shaft containing a center circular hole and a crack

0.5, 0.6, 0.7, respectively. The results of D^* for different values of a_2/R_0 are given in Fig.15. It is found that with the larger ratio of l/R_0, the loss of relative D^* changes greater. The non-dimensional stress intensity factors $K_{\mathrm{III}}^*(c)$ and $K_{\mathrm{III}}^*(d)$ for different values of a_2/R_0 are shown in Fig.16, which shows that when the crack length approaches the edge of the center hole and boundary of the shaft, $K_{\mathrm{III}}^*(c)$ and $K_{\mathrm{III}}^*(d)$ sharply increase due to the interaction.

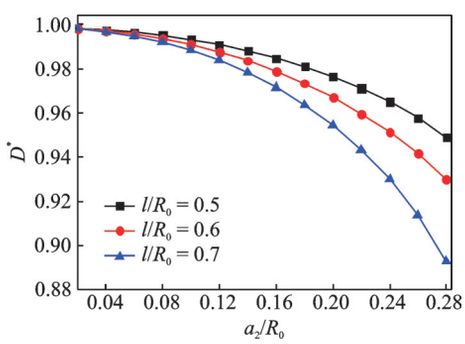

Fig.15 Non-dimensional torsional rigidity D^* versus a_2/R_0

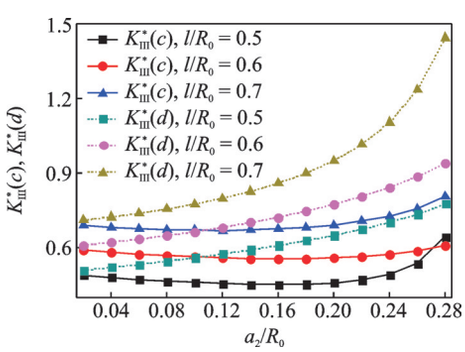

Fig.16 Non-dimensional intensity factor $K_{\mathrm{III}}^*(c)$ and $K_{\mathrm{III}}^*(d)$ versus a_2/R_0

4 Conclusions

We studied the Saint-Venant's torsion of a circular shaft with multiple elliptical inclusions with different material constants from the matrix. Based on the complex variable method, the complex potentials are expressed in the form of Faber series, and then their unknown coefficients are solved by the continuous conditions at the interface between the matrix and inclusions. Solutions for the cases of multiple circular inclusions/elliptic holes/cracks can be easily obtained as special cases of the present work, and they are compared with previous results obtained based on the integral equation method, the null-field integral approach or other numerical methods. It is shown that the present work has advantages such as high accuracy and good convergence. Furthermore, several numerical examples for the interaction between multiple elliptical inclusions/holes/cracks are presented to discuss the effects of the parameters of these defects on the stress, torsional rigidity and the stress intensity factors, and it is found that the geometry size, material constants and locations of the defects play a significant role in these variables of fields.

References

[1] LING C B. Torsion of a circular tube with longitudinal circular holes[J]. Quarterly of Applied Mathematics, 1947, 5: 168-181.

[2] HOWLAND R C J. Potential functions with periodicity in one coordinate[J]. Mathematical Proceedings of The Cambridge Philosophical Society, 1934, 30: 315-326.

[3] KUO Y M, CONWAY H D. The torsion of composite tubes and cylinders[J]. International Journal of Solids And Structures, 1973, 9: 1553-1566.

[4] KUO Y M, CONWAY H D. Torsion of cylinders with multiple reinforcement[J]. Journal of the Engineering Mechanics Division, 1974, 100(2): 221-234.

[5] JASWON M A, PONTER A R S. An integral equation solution of the torsion problem[J]. Royal Society of London, 1963, 273: 237-246.

[6] GAO C F, MENG L C, SHI Y. Coupled FEM analyses on electro-mechanical problem of electrostrictive plate with elliptical hole[J]. Transactions of Nanjing University of Aeronautics and Astronautics, 2014, 31(5): 589-598.

[7] KATSIKADELIS J T, SAPOUNTZAKIS E J. Torsion of composite bars by boundary element method[J]. Journal of Engineering Mechanics, 1985, 111: 1197-1210.

[8] SPOUNTZAKIS E J, MOKOS V G. Nonuniform torsion of composite bars by boundary element method[J]. Journal of Engineering Mechanics, 2001, 127: 945-953.

[9] LI Z X, KO J M, NI Y Q. Torsional rigidity of reinforced concrete bars with arbitrary sectional shape[J]. Finite Elements in Analysis and Design, 2000, 35: 349-361.

[10] CHEN J T, SHEN W C, CHEN P Y. Analysis of circular torsion bar with circular holes using null-field approach[J]. Computer Modeling in Engineering & Sciences, 2006, 12: 109-119.

[11] CHEN J T, LEE Y T. Torsional rigidity of a circular bar with multiple circular inclusions using the null-field integral approach[J]. Computational Mechanics, 2009, 44: 221-232.

[12] ECSEDI I, BAKSA A. Prandtl's formulation for the Saint-Venant's torsion of homogeneous piezoelectric beams[J]. International Journal of Solids and Structures, 2010, 47: 3076-3083.

[13] ECSEDI I, BAKSA A. Saint-Venant torsion of non-homogeneous orthotropic circular cylinder[J]. Archive of Applied Mechanics, 2020, 90: 815-827.

[14] WANG X, SCHIAVONE P. Torsion of an arbitrarily shaped nanosized bar[J]. Archive of Applied Mechanics, 2016, 86:1037-1048.

[15] HASSANI A, FAAL R T. Saint-Venant torsion of orthotropic bars with a circular cross-section containing multiple cracks[J]. Mathematics and Mechanics of Solids, 2016, 21(10): 1198-1214.

[16] MUSKHELISHVILI N I. Some basic problem of the mathematical theory of elasticity[M]. Groningen: Noordhoof International Publishing, 1975.

[17] YUE J C, TANG R J. Integral equation method for the torsion of a composite cylinder with crack and inclusion[J]. Engineering Fracture Mechanics, 1996, 55: 763-775.

[18] DAI M, SCHIAVONE P, GAO C F. Prediction of the stress field and effective shear modulus of composites containing periodic inclusions incorporating interface effects in anti-plane shear[J]. Journal of Elasticity, 2016, 125(2): 217-230.

[19] YANG H B, DAI M, GAO C F. Stress field in a porous material containing periodic arbitrarily-shaped holes with surface tension[J]. Mathematics and Mechanics of Solids, 2018, 23(1): 120-130.

[20] CURTISS J H. Faber polynomials and the Faber series[J]. The American Mathematical Monthly, 1971, 78: 577-596.

[21] XU X W, MAN H C, YUE T M. Strength prediction of composite laminates with multiple elliptical holes[J]. International Journal of Solids and Structures, 2000, 37: 2887-2900.

[22] KOSMODAMIANSKII A S, KALOEROV S A. Thermal stress in connected multiply plates[M]. Kiev: Vishcha Shkola, 1983.

Acknowledgements This work was supported by the National Natural Science Fund of China (No. 11802040) and the Natural Science Foundation of the Jiangsu Higher Education Institutions of China (No.18KJB130001).

Author Dr. **HUANG Cheng** received the B.S. and Ph.D. degrees in solid mechanics from Nanjing University of Aeronautics and Astronautics, Nanjing, China, in 2010 and 2017, respectively. From 2017 to present, he has been with the School of Aviation and Mechanical Engineering, Changzhou Institute of Technology. His research is focused on mechanics of smart materials and structures.

Author contributions Prof. **GUO Hun** designed the study. Dr. **HUANG Cheng** wrote the manuscript. Dr. **YIN Maoshu** and Mr. **QI Xiao** carried out calculations and analyses. All authors commented on the manuscript draft and approved the submission.

Competing interests The authors declare no competing interests.

(Production Editor: ZHANG Huangqun)

含椭圆夹杂或裂纹的圆柱扭转问题研究

黄 成[1], 殷茂淑[2], 祁 霄[1], 郭 魂[1]

(1.常州工学院航空与机械工程学院,常州 213032,中国;
2.上海空间电源研究所物理电源事业部,上海 200240,中国)

摘要:基于复势函数理论,提出了一种简明的方法来研究含多个椭圆夹杂或裂纹圆柱体的Saint-Venant扭转问题。首先,应用Faber级数展开,导出了具有N个椭圆夹杂圆柱体的复势函数表达,然后计算圆柱体内部的切应力和扭转刚度。当椭圆夹杂退化为裂纹时,获得裂纹尖端应力强度因子解。最后,通过数值算例与已有文献结果对比验证了本文方法的正确性,并进一步讨论了几何参数、不同软硬夹杂相对基体的剪切模量比和椭圆夹杂或裂纹的阵列形式对局部应力场的影响。通过数值分析表明本文方法具有精度高、收敛性好等优点。

关键词:Saint-Venant扭转;复势函数方法;Faber级数